Room-Temperature Polariton Parametric Scattering Driven by a One-Dimensional Polariton Condensate

Wei Xie, Hongxing Dong, Saifeng Zhang, Liaoxin Sun, Weihang Zhou, Yanjing Ling, Jian Lu, Xuechu Shen,* and Zhanghai Chen†

State Key Laboratory of Surface Physics, Key Laboratory of Micro and Nano Photonic Structures (Ministry of Education), Department of Physics, Fudan University, Shanghai 200433, China

(Received 30 November 2011; published 18 April 2012)

We demonstrate a novel way to realize room-temperature polariton parametric scattering in a one-dimensional ZnO microcavity. The polariton parametric scattering is driven by a polariton condensate, with a balanced polariton pair generated at the adjacent polariton mode. This parametric scattering is experimentally investigated by the angle-resolved photoluminescence spectroscopy technique under different pump powers and it is well described by the rate equation of interacting bosons. The direct relation between the intensity of the scattered polariton signal and that of the polariton reservoir is acquired under nonresonant excitation, exhibiting the explicit nonlinear characteristic of this room-temperature polariton parametric process.

DOI: 10.1103/PhysRevLett.108.166401 PACS numbers: 71.36.+c, 42.65.−k, 78.66.Hf

Exciton-polaritons are bosonic excitations formed by the strong coupling between excitons and photons [1,2]. Unique scattering processes can occur through the interaction among the excitonic components of the half-light, half-matter quasiparticles [3]. These scatterings are responsible for the energy relaxation, thermalization [4], and nonlinearities of polaritons. Great effort has been devoted to the study of polariton nonlinear scatterings in the last decades. The stimulated polariton scattering to the final state has been used to realize the polariton laser [5]. Polariton parametric scattering (PPS) processes have been achieved in microcavities [6–14], and lead to many interesting macro-quantum phenomena, such as the polariton superfluidity [15], condensate, vortices [16], etc.

High-density polariton gases (HPGs) are indispensable to optical nonlinearities of polaritons. One usually uses external lasers to resonantly excite the HPGs for the studies of optical nonlinearities. An alternative way to obtain HPGs is to utilize the gain mechanism of polariton condensation. In this mechanism, polaritons are scattered to some final states and accumulate when the stimulated process occurs under nonresonant excitation [17]. These coherent polaritons [18] are ideal scattering sources for the PPS processes. Compared with the conventional method of resonant pumping at the specific incident angle, this approach is much easier to operate because of nonresonant excitation. Moreover, the polariton condensate at the lowest energy state easily induces interbranch PPS and generates balanced signal and idler beams [19]. These balanced polariton pairs are intrinsically quantum entangled, making them ideal candidates for quantum correlation and information application such as quantum cryptography, etc. However, so far, experimental work regarding such polariton condensate induced interbranch PPS is yet to be demonstrated.

From the application point of view, the operation temperature of PPS is crucial. In the work of Ref. [20], polariton parametric amplification was achieved at 220 K in a CdTe planar microcavity. However, the temperature upper limit is expected to be above room temperature for some wide bandgap semiconductors like ZnO and GaN. The large exciton binding energy and oscillator strength in these materials enable polaritons to remain stable at room temperature [21]. Furthermore, in the one-dimensional (1D) microcavity systems based on these materials, a variety of scattering channels are available for PPSs due to their multiplet of subbranches [22]. And the intersubbranch PPS processes are more efficient in 1D microcavities than in planar microcavities because of the favorable configurations for momentum conservation [23]. However, to our knowledge, the characteristics of room-temperature PPS in 1D microcavity systems remain unexplored until now.

In this work, we demonstrate a room-temperature PPS process driven by a polariton condensate in a ZnO 1D microcavity. The scattering source, i.e., the polariton condensate, is generated by nonresonant excitation. Scatterings to the adjacent polariton mode are amplified when the excitation power exceeds the threshold, leading to an intersubbranch PPS in this 1D microcavity. The signal and idler are balanced polariton pairs with degenerate energy and opposite momenta.

The samples used in our experiments are ZnO microwires fabricated by a carbothermal method. Figure 1(a) is the scanning electron microscope image of a typical ZnO microwire, showing smooth facets and a regular hexagonal cross section. The ZnO microwire is a uniaxial crystal with an optical axis (**c** axis) perpendicular to its hexagonal plane. It is found that such a microwire can be used as a whispering gallery type optical resonator [24] with a high

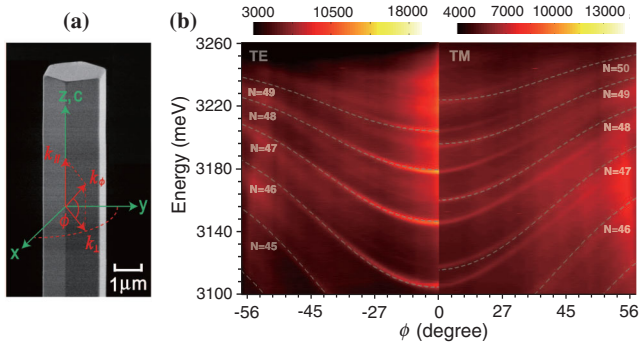

FIG. 1 (color). (a) Scanning electron microscope image of a single ZnO microwire. **c**: the crystallographic axis. (b) The angle-resolved photoluminescence spectral ($\boldsymbol{k}$-space) mapping under cw excitation. Both TE (electric field component of light $\vec{\varepsilon} \perp \mathbf{c}$) and TM ($\vec{\varepsilon} \parallel \mathbf{c}$) polarized polariton modes in the ZnO microcavity are shown. Dashed curves: Theoretical fittings for the lower polariton branches. The photon emitted at angle ϕ carries the polariton energy E and its wave vector component $k_{\parallel} = (E/\hbar c)\sin\phi$.

quality factor Q several times larger than that of the ZnO planar microcavity. This whispering gallery microcavity provides two-dimensional confinement for photons, leading to a one-dimensional optical system. With an angle-resolved photoluminescence (PL) spectroscopy technique, it has been demonstrated that the strong coupling between exciton and photon (i.e., exciton-polariton) can be realized in such microcavities [25,26]. Figure 1(b) shows the energy dispersions of the polariton lower branches for a ZnO microwire with the radius being 1.45 μm, under continuous He-Cd laser (325 nm) excitation. The dispersion curvatures for both TE and TM polarizations tend to be smaller and smaller at large angles, showing the typical repulsion-like behavior of strong coupling. These dispersions can be well described by the coupled oscillator model, as illustrated in Fig. 1(b) (dashed curves), and the Rabi splitting obtained is as large as 300 meV.

Under high excitation, exciton-polaritons show nonlinear characteristics at room temperature. The excitation source is a Nd:YAG pulsed laser (wavelength: 355 nm, pulse width: 3 ns, repetition rate: 10 Hz) with a spot size of $\sim 10\ \mu\mathrm{m}^2$, which can create high-density carriers in the ZnO microcavity. When the excitation power exceeds a certain threshold ($P = 0.33\ \mu$W), the lowest energy states ($\boldsymbol{k}_{\parallel} = 0$) of the $N = 47, 48$ polariton modes are remarkably populated, and lasing phenomena [27] from these two TE polarized polariton modes are observed, as shown in Fig. 2(a). Interestingly, when the pumping power further increases, there appear two bright spots degenerate in energy with their lasing source and located symmetrically at the dispersion curve of the adjacent polariton mode, as shown in Fig. 2(b). The intensities of these spots (~ 5000 for the mode $N = 48$ and $\sim 30\,000$ for the mode $N = 47$, $P = 1.30\ \mu$W) are much larger than that of the background polariton modes (~ 500) without the contribution of scattering. This characteristic indicates that the two bright spots are induced by the intersubbranch PPS, as shown schematically in Fig. 2(c). The balanced signal and idler have degenerate energy and opposite momenta, with the polarizations being the same as that of the scattering source. One can describe the scattering process with $\{[E, \boldsymbol{k}(0)], [E, \boldsymbol{k}(0)]\}_N \rightarrow \{[E, \boldsymbol{k}(\phi)], [E, \boldsymbol{k}(-\phi)]\}_{N-1}$.

To further study the underlying physics, we carried out power-dependent experiments on this nonlinear scattering process. Four typical $\boldsymbol{k}$-space PL mappings under different excitation powers are shown in Fig. 3(a). Here, we study the scattering probabilities to the signal beam, i.e., at the positions B and B' (the scattering to the idler beam has a similar behavior). For comparisons, the off-resonance positions (marked A, A', C, C') are also selected. The intensity ratios I/I_0 at positions A, B, and C have been plotted in Fig. 3(b), as functions of the intensity of scattering source I_0. The nonlinearity of the scatterings to the on-resonance position B is unambiguously demonstrated, while scatterings to the off-resonance positions (A and C) show nearly

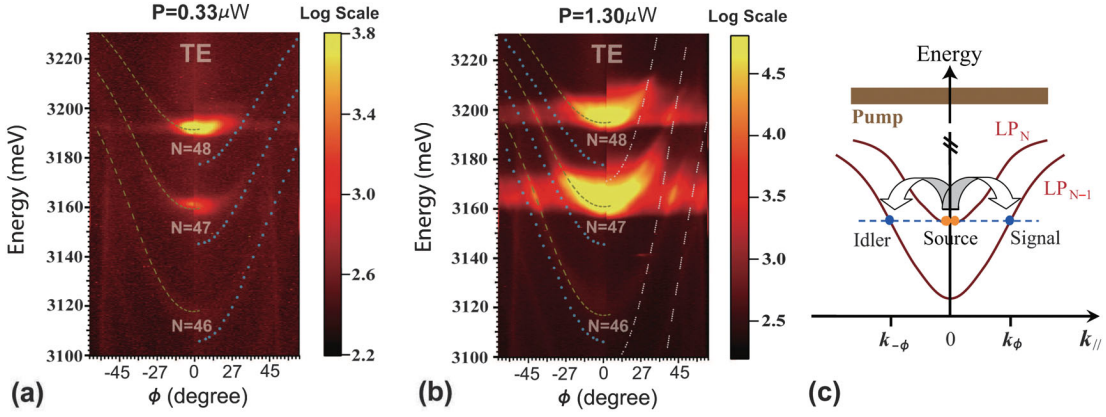

FIG. 2 (color). Room-temperature $\boldsymbol{k}$-space PL mapping under high excitation. (a) Polariton lasing in the 1D microcavity with pumping power $P = 0.33\ \mu$W. The intensity has been color scaled in logarithm. (b) Polariton nonlinear scatterings with pumping power $P = 1.30\ \mu$W. (c) Schematic picture for the PPS process, $\{[E, \boldsymbol{k}(0)], [E, \boldsymbol{k}(0)]\}_N \rightarrow \{[E, \boldsymbol{k}(\phi)], [E, \boldsymbol{k}(-\phi)]\}_{N-1}$.

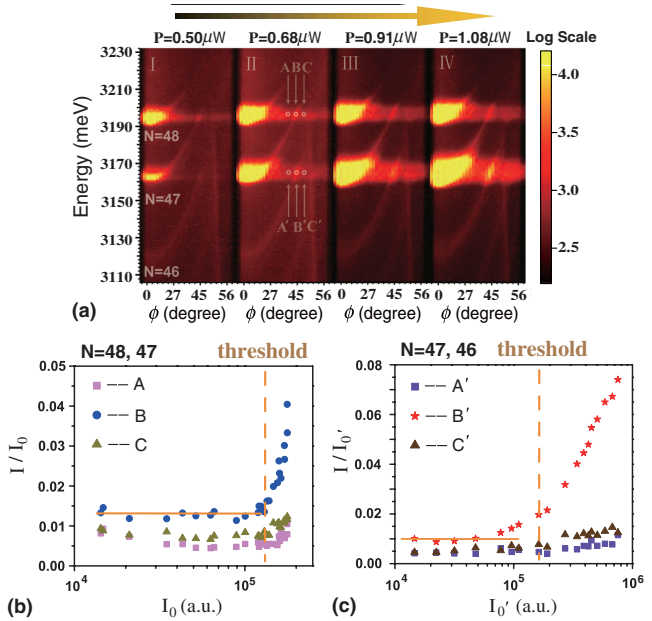

FIG. 3 (color). (a) $\boldsymbol{k}$-space PL mappings under four different pumping powers. (b) Scattering probabilities at positions *A, B, C* as a function of the intensity of the polariton scattering source. *B*: Scattering to the $N = 47$ polariton mode, *A* and *C*: Off-resonance scatterings. (c) The similar scattering behavior between polariton modes $N = 47$ and $N = 46$.

linear characteristics. The linear scatterings to those off-resonance positions are attributed to the polariton scatterings by the static disorder in the sample, with random scattering directions [28]. The "scattering belt," i.e., the red zonal area extending from the scattering source [see in Fig. 3(a)], is a clear manifestation of the normal Rayleigh scattering. On the other hand, the nonlinear scattering to position *B* confirms the intrinsic threshold characteristic of PPS, and the discontinuous derivative of the scattering probability at the threshold [see in Fig. 3(b)] shows the peculiar feature of PPS: a second-order phase transition [11]. These properties distinguish the intersubbranch PPS from the polariton-disorder scattering. In addition, a similar behavior is observed for the scattering process between modes $N = 47$ and $N = 46$, but with a lower scattering gain, as depicted in Fig. 3(c). This difference could probably be ascribed to a smaller excitonic fraction of the polariton condensate at mode $N = 47$ ($\sim 45\%$ at the $k_{\parallel} = 0$ polariton state for the mode $N = 47$, while $\sim 56\%$ for the mode $N = 48$).

Theoretically, the dynamics of polariton scattering processes can be described by the rate equation of interacting bosons [3]. A schematic diagram is shown in Fig. 4(a). In this model, the polariton occupation number of the scattering source n_0 is determined by the following physical processes: the effective injection by the gain mechanism of polariton condensate (with injection rate P_0), the loss by scatterings (with scattering coefficient α) and other damping processes (with damping coefficient γ_0): radiative recombination, some nonradiative relaxation channels like interactions with phonons, etc. For the signal n_S and idler n_I, the polariton populations are mainly determined by the scattering from polariton reservoirs and their damping processes (with damping coefficients γ_S, γ_I, respectively). Direct injection from the exciton bath is ignored, considering the fact that the contribution from the background polariton mode is negligibly small, as mentioned above. In this model, both the linear polariton-disorder scattering (Δn_{linear}) and PPS (Δn_{PPS}) have been taken into account. Considering the bosonic characteristic of polaritons and the symmetry of signal and idler, the time evolution of signal population can be described as follows:

$$\frac{dn_S}{dt} = -\gamma_S n_S + \Delta n_{\text{PPS}} + \Delta n_{\text{linear}}, \tag{1}$$

$$\Delta n_{\text{PPS}} = \alpha_{\text{PPS}} n_0^2 (n_S + 1)^2 - \alpha_{\text{PPS}} n_S^2 (n_0 + 1)^2, \tag{2}$$

$$\Delta n_{\text{linear}} = \alpha_{\text{linear}} n_0 (n_S + 1) - \alpha_{\text{linear}} n_S (n_0 + 1), \tag{3}$$

where α_{PPS} is the scattering coefficient for the PPS process, and α_{linear} corresponds to the coefficient of polariton-disorder scattering. Because polariton-polariton scattering is a transient process and the time for building up PPS gain ($\sim$ ps) [7] is much smaller than the laser pulse width ($\sim$ ns), it is reasonable to consider that the system reaches a steady state. By seeking the stationary solution of the rate equation, we deduce the polariton occupation number of the signal state n_S (idler n_I) as a function of the scattering source population n_0, which is used in the following fittings.

The experimental data of the scattered signal $I_S(I_{S'})$ versus the scattering source $I_0(I_{0'})$ are shown in Figs. 4(b) and 4(c). Unlike traditional PPSs by resonant excitation, the PL intensity of polariton reservoirs does not mix up with the light signal from the pumping laser in our case. Thus, the direct relationship between the intensity of scattered polariton signal I_S and that of the scattering source I_0 can be experimentally investigated, which is different from its dependence on the polariton injection rate P_0 (or the laser power). In addition, the approximately equal intensity and the same variation trend of signal and idler confirm that this interbranch PPS process generates balanced polariton pairs. The PL intensity is proportional to the polariton population, and the scaling coefficient is determined by setting $n_S = 1$ at the threshold of PPS [3]. The damping coefficient γ_S is extracted ($\hbar\gamma_S \sim 3$ meV) under low excitation conditions when polariton scatterings can be ignored. For the scattering between modes $N = 48$ and $N = 47$, the fitting of this PPS process with $\hbar\alpha_{\text{PPS}} = 1.1 \times 10^{-4}$ meV is shown in Fig. 4(b) (see the blue line), which agrees well with our experimental data (for both signal and idler). A similar fitting is carried out for the scattering process between modes $N = 47$ and $N = 46$, with a smaller scattering coefficient $\hbar\alpha_{\text{PPS}} = 0.3 \times 10^{-4}$ meV, as shown

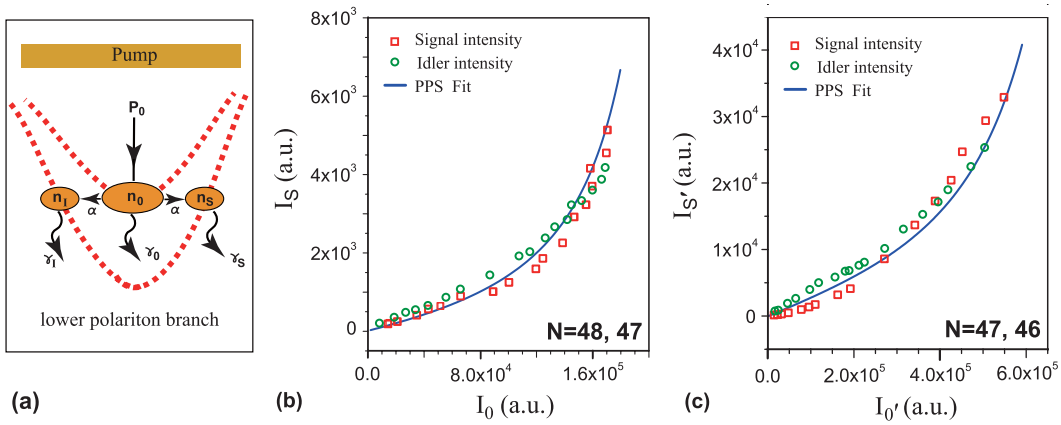

FIG. 4 (color). (a) Sketch for the dynamics of the PPS process. (b) Theoretical fitting for the scattering between modes $N = 48$ and $N = 47$. The red diamonds (green circles) represent the dependence of the scattered polariton signal I_S (idler I_I) on the scattering source I_0. The blue line is the fitting of the PPS process with $\hbar\alpha_{\mathrm{PPS}} = 1.1 \times 10^{-4}$ meV. (c) Similar fitting for the scattering between modes $N = 47$ and $N = 46$ with $\hbar\alpha_{\mathrm{PPS}} = 0.3 \times 10^{-4}$ meV. The polariton-disorder scattering coefficients $\hbar\alpha_{\mathrm{linear}}$ for these two scattering processes are of the order of 10^{-2} meV.

in Fig. 4(c). The polariton-polariton scattering coefficient α_{PPS} here is expected to be smaller, as the excitonic fraction of the scattering polaritons is less [3]. At the threshold of PPS, the polariton population n_0^{thr} can be expressed as $\sqrt{\gamma_S/2\alpha_{\mathrm{PPS}}}$ [3], and the polariton-polariton interaction coefficient $M_{\mathrm{pp}} = (S/\pi\lambda_B^2)\hbar\gamma_S/n_0^{\mathrm{thr}}$ [11] can be acquired in units of λ_B, where S is the area of the hexagonal cross section of the ZnO microwire and λ_B is the Bohr radius of the exciton. With the value of this interaction coefficient, the density of polaritons can be estimated: $\rho = (\Delta E/M_{\mathrm{pp}})/(\frac{4}{3}\pi\lambda_B^3)$, where ΔE is the energy blueshift of polaritons in present density surroundings. In our system, the polariton energy blueshift from the low excitation power to the PPS threshold is $\sim$18 meV; hence, the polariton density is $\sim 10^{17}$ cm^{-3} at the threshold, which is still smaller than the Mott density ($\sim 10^{19}$ cm^{-3}) for the ZnO system [29].

The nonlinear scattering processes discussed above occur at high excitation conditions; it is thus necessary to confirm that the system is still in the strong coupling regime. Besides the estimated polariton density, there is other evidence to support this view. The blue dotted curves in Figs. 2(a) and 2(b) show the well-defined polariton dispersion curves, which are extracted from the mappings under low excitation conditions by the continuous laser. Obviously, the dispersion curves under high excitations resemble those obtained under low excitations, with a small energy blueshift ($\sim$ 18 meV, one-fifteenth of the Rabi splitting) originating from the polariton-polariton interaction, as mentioned above. Moreover, these dispersions under high excitation can also be well fitted by the coupled oscillator model when the polariton-polariton interaction is taken into account (the green short-dashed curves). For comparison, the theoretical dispersions of pure optical cavity modes are also depicted in Figs. 2(a) and 2(b) (the white long-dashed curves), showing a large deviation from our experimental dispersion curves. Therefore, one can conclude that the strong coupling between excitons and photons is still maintained under such excitation conditions.

In summary, we have reported the first experimental observation of room-temperature PPS in a one-dimensional ZnO whispering gallery microcavity. Unlike conventional PPS processes, the scatterings in our work are driven by a polariton condensate under nonresonant excitation conditions. Thanks to the multiplet subbranches in this 1D microcavity, an intersubbranch scattering channel is available and balanced polariton pairs are generated at room temperature. The direct relation between the intensity of the scattered polariton signal and that of the scattering source is acquired, and the dynamics of this parametric scattering process is well described by the rate equation of interacting bosons. Our work opens a new way for the generation of scattering sources in PPS and is promising for the development of polariton parametric process applications at room temperature.

The work is funded by the 973 projects of China (No. 2011CB925600), NSFC (No. 91121007), and the International Science and Technology Cooperation Program (No. 2010DFA02600). The authors acknowledge fruitful discussions with Professor Le Si Dang and Professor Jacqueline Bloch.

*xcshen@fudan.edu.cn
†zhanghai@fudan.edu.cn

[1] J. J. Hopfield, Phys. Rev. **112**, 1555 (1958).
[2] C. Weisbuch, M. Nishioka, A. Ishikawa, and Y. Arakawa, Phys. Rev. Lett. **69**, 3314 (1992).

[3] A. V. Kavokin and G. Malpuech, Cavity Polaritons 32 (Elsevier, Amsterdam, 2003).
[4] J. Kasprzak, D. D. Solnyshkov, R. André, Le Si Dang, and G. Malpuech, Phys. Rev. Lett. **101**, 146404 (2008).
[5] R. Huang, F. Tassone, and Y. Yamamoto, Phys. Rev. B **61**, R7854 (2000).
[6] M. Kuwata-Gonokami, S. Inouye, H. Suzuura, M. Shirane, R. Shimano, T. Someya, and H. Sakaki, Phys. Rev. Lett. **79**, 1341 (1997).
[7] P. G. Savvidis, J. J. Baumberg, R. M. Stevenson, M. S. Skolnick, D. M. Whittaker, and J. S. Roberts, Phys. Rev. Lett. **84**, 1547 (2000).
[8] G. Messin, J. Ph. Karr, A. Baas, G. Khitrova, R. Houdré, R. P. Stanley, U. Oesterle, and E. Giacobino, Phys. Rev. Lett. **87**, 127403 (2001).
[9] P. G. Savvidis, C. Ciuti, J. J. Baumberg, D. M. Whittaker, M. S. Skolnick, and J. S. Roberts, Phys. Rev. B **64**, 075311 (2001).
[10] S. Kundermann, M. Saba, C. Ciuti, T. Guillet, U. Oesterle, J. L. Staehli, and B. Deveaud, Phys. Rev. Lett. **91**, 107402 (2003).
[11] C. Ciuti, P. Schwendimann, and A. Quattropani, Semicond. Sci. Technol. **18**, S279 (2003).
[12] G. Dasbach, C. Diederichs, J. Tignon, C. Ciuti, Ph. Roussignol, C. Delalande, M. Bayer, and A. Forchel, Phys. Rev. B **71**, 161308(R) (2005).
[13] C. Diederichs, J. Tignon, G. Dasbach, C. Ciuti, A. Lemaître, J. Bloch, Ph. Roussignol, and C. Delalande, Nature (London) **440**, 904 (2006).
[14] M. Romanelli, C. Leyder, J. Ph. Karr, E. Giacobino, and A. Bramati, Phys. Rev. Lett. **98**, 106401 (2007).
[15] A. Amo *et al.*, Nature (London) **457**, 291 (2009).
[16] D. Sanvitto *et al.*, Nature Phys. **6**, 527 (2010).
[17] S. Christopoulos *et al.*, Phys. Rev. Lett. **98**, 126405 (2007).
[18] F. P. Laussy, G. Malpuech, A. Kavokin, and P. Bigenwald, Phys. Rev. Lett. **93**, 016402 (2004).
[19] M. Abbarchi, V. Ardizzone, T. Lecomte, A. Lemaître, I. Sagnes, P. Senellart, J. Bloch, P. Roussignol, and J. Tignon, Phys. Rev. B **83**, 201310(R) (2011).
[20] M. Saba *et al.*, Nature (London) **414**, 731 (2001).
[21] M. Zamfirescu, A. Kavokin, B. Gil, G. Malpuech, and M. Kaliteevski, Phys. Rev. B **65**, 161205(R) (2002).
[22] G. Dasbach, M. Schwab, M. Bayer, D. N. Krizhanovskii, and A. Forchel, Phys. Rev. B **66**, 201201(R) (2002).
[23] C. Ciuti, Phys. Rev. B **69**, 245304 (2004).
[24] T. Nobis, E. M. Kaidashev, A. Rahm, M. Lorenz, and M. Grundmann, Phys. Rev. Lett. **93**, 103903 (2004).
[25] L. Sun, Z. Chen, Q. Ren, K. Yu, L. Bai, W. Zhou, H. Xiong, Z. Q. Zhu, and X. Shen, Phys. Rev. Lett. **100**, 156403 (2008).
[26] A. Trichet, L. Sun, G. Pavlovic, N. A. Gippius, G. Malpuech, W. Xie, Z. Chen, M. Richard, and Le Si Dang, Phys. Rev. B **83**, 041302(R) (2011).
[27] L. Sun, S. Sun, H. Dong, W. Xie, M. Richard, L. Zhou, L. S. Dang, X. Shen, Z. Chen *et al.*, arXiv:1007.4686.
[28] W. Langbein and J. M. Hvam, Phys. Rev. Lett. **88**, 047401 (2002).
[29] Y. Chen, N. T. Tuan, Y. Segawa, H.-j. Ko, S.-k. Hong, and T Yao, Appl. Phys. Lett. **78**, 1469 (2001).